International Immunopharmacology 80 (2020) 106141

Contents lists available at ScienceDirect

International Immunopharmacology

journal homepage: www.elsevier.com/locate/intimp

MicroRNA-152 attenuates neuroinflammation in intracerebral hemorrhage by inhibiting thioredoxin interacting protein (TXNIP)-mediated NLRP3 inflammasome activation

Liuting Hu[a], Heyu Zhang[b], Bingyang Wang[a], Qiang Ao[c], Zhiyi He[a,*]

[a] Department of Neurology, The First Affiliated Hospital of China Medical University, Shenyang 110000, People's Republic of China
[b] Department of Neurology, The First Affiliated Hospital Sun Yat-sen University, Guangzhou 510080, People's Republic of China
[c] Department of Tissue Engineering, China Medical University, Shenyang 110122, People's Republic of China

ARTICLE INFO

Keywords:
Intracerebral hemorrhage
Neuroinflammation
MicroRNA-152
TXNIP
NLRP3 inflammasome

ABSTRACT

Neuroinflammation significantly contributes to brain injury and neurological deterioration following intracerebral hemorrhage (ICH). MicroRNA-152(miR-152) was reported to be downregulated in ICH patients and to possess anti-inflammatory properties in other diseases. In this study, we aimed to explore the role of miR-152 in ICH, and the underlying mechanisms, using a collagenase-induced rat ICH model and hemin-exposure as a cell model. We first confirmed that miR-152 was consistently downregulated in both models. Overexpression of miR-152 in microglial BV2 cells reduced hemin-induced inflammatory response and reactive oxygen species (ROS) generation, thus protecting co-cultured neuronal HT22 cells. Moreover, overexpression of miR-152 by intracerebroventricular lentivirus injection in ICH rats significantly alleviated neurodecifits, brain edema, and hematoma. These changes were associated with a marked reduction in ICH-induced neuronal death, as detected by co-staining of NeuN and TUNEL, and ICH-induced neuroinflammation, as revealed by inflammatory cytokine levels as well as by the number of Iba1 positive-stained cells in the perihematomal region. Mechanistically, miR-152 significantly inhibited ICH-induced TXNIP expression, and its overexpression blocked the interaction between TXNIP and NOD-like receptor pyrin domain containing 3(NLRP3), thus inhibiting NLRP3-driven inflammasome activation to attenuate neuroinflammation *in vivo* and *in vitro*. Moreover, the results of si-TXNIP transfection further confirmed that TXNIP inhibition was involved in the reduction of NLRP3 inflammasome activation by the overexpression of miR-152. Collectively, the present study demonstrates that miR-152 confers protection against ICH-induced neuroinflammation and brain injury by inhibiting TXNIP-mediated NLRP3 inflammasome activation, indicating a potential strategy for ICH treatment.

1. Introduction

Intracerebral hemorrhage (ICH), associated with high mortality and disability, is a common and devastating subtype of stroke [1,2], occurring when blood vessels rupture within the brain. However, effective therapeutic treatments are not available, because of the complex pathogenesis of ICH [3]. The ICH pathogenic processes can be classified into two major phases, namely primary and secondary brain injury. The former arises from intraparenchymal hematoma, while the latter results from the products of red blood cell lysis, leading to cytotoxicity, excessive oxidative stress, and neuroinflammation in the perihematomal region [4,5]. Thus, timely and effective targeted therapeutic treatments should be further explored.

Among the above-mentioned factors contributing to secondary brain injury, neuroinflammation is considered a key contributor [6,7]. Neuroinflammation, evoked by the hematoma degradation products, involves microglia activation, systemic immune cell infiltration, production of pro-inflammatory cytokines, and ROS generation, and contributes to neuronal death, edema exacerbation, and poor prognosis [8]. In addition, increasing evidence indicates that treatments targeting neuroinflammation can alleviate ICH-induced brain injury to some extent [9–11].

MicroRNAs (miRNAs) are a class of noncoding RNAs that participate in various pathophysiological processes, and function by down-regulating gene expression through their binding to the 3'UTR of the target mRNAs [12]. Accumulating studies have shown that miRNAs

* Corresponding author at: Department of Neurology, The First Affiliated Hospital of China Medical University, 155N, Nanjing Street, Heping District, Shenyang 110000, People's Republic of China.
E-mail address: hezhiyi0301@sina.com (Z. He).

https://doi.org/10.1016/j.intimp.2019.106141
Received 21 October 2019; Received in revised form 30 November 2019; Accepted 19 December 2019

play a critical role in regulating neuroinflammation in ICH. Wang et al. [13] reported that miR-140-5p attenuated neuroinflammation in ICH by targeting TLR4. In addition, miR-124 was found to confer protection from brain inflammation by modulating microglia polarization toward the M2 phenotype [14]. MiR-152 is a tumor suppressor miRNA that has been widely studied in tumor biology [15–17]. Recently, several researchers have investigated its role in inflammatory modulation. For example, miR-152 exerted an anti-inflammatory effect in lipopolysaccharide (LPS)-stressed macrophages [18], inhibited the inflammatory response in a mouse model of spinal cord injury (SCI)[19], and negatively regulated the innate response and inhibited the cytokines production of dendritic cells induced by TLR3, TLR4 and TLR9 agonists [20]. However, whether miR-152 is involved in the neuroinflammation modulation of ICH is still unclear. Moreover, in our previous miRNA array chip data, miR-152 was downregulated in the serum of ICH patients [21], but the significance of such downregulation has not been explored.

This study aims to explore the role of miR-152 in ICH and its underlying molecular basis, using a rat model of ICH and hemin-exposure in a cell model for *in vivo* and *in vitro* studies, respectively.

2. Materials and methods

2.1. Animal preparation

All experimental protocols involving animals were conducted in accordance with National Institutes of Health Guide for the Care and Use of Laboratory Animals and the Animal Research: Reporting of In Vivo Experiments (ARRIVE) guidelines.

Male Wistar rats weighing 250–280 g were obtained from Liaoning Changsheng Biotechnology Co. Ltd (China). All animals were allowed free access to food and water and were maintained under controlled temperature and light/dark cycles. Sodium pentobarbital was used for animal anesthesia. All experimental procedures were approved by the Animal Care Committee of China Medical University (2012-38-1).

2.2. Experimental design

To study whether miR-152 is dysregulated in ICH rats, 48 rats were randomly assigned into four group (twelve rats per group):sham group, first day post-ICH group, third day post-ICH group, and fifth day post-ICH group. Six rats in each group were decapitated at the respective time point to collect brain tissue to measure miR-152 expression, and serum samples for testing inflammatory cytokines; the remaining six rats per group were perfused with fixative for histological analysis.

To investigate the effects of miR-152 on ICH, another set of animals were randomly assigned to four groups (twenty-four rats per group):-sham group, ICH group, ICH + lentivirus-miRNA negative control (LV-miR-NC) group, and ICH + lentivirus-miR-152 (LV-miR-152) group. Six rats per group were evaluated for neurological function on the first, third, and fifth day after ICH. The others were killed on the third day after ICH: Six per group were used for brain water content measurements, six were perfused with fixative for histological analysis, including Iba1 staining and TUNEL staining, and the remaining six were decapitated to collect brain tissue for RT-qPCR and western blotting, and collecting serum samples for pro-inflammatory cytokines assay.

2.3. Intracerebroventricular lentivirus injection and establishment of a rat ICH model

The intracerebroventricular injection of lentivirus were conducted according to the previous study [22]. Briefly, rats were placed on a stereotaxic frame under anesthesia, a 1 mm cranial burr hole was drilled and 5ul LV-miR-152 or LV-miR-NC (10^9 transfection unit/ml), constructed by GeneChem Company (China), was slowly injected into the right lateral ventricle by using microsyringe (stereotaxic coordinates were 1.5 mm posterior, 1.8 mm lateral, and 3.5 mm below the horizontal plane of bregma). To prevent reflux or backflow, the microsyringe was slowly withdrawn 5 min after the injection, and the cranial burr hole was sealed with bone wax.

Two weeks later, the rat ICH model induced by collagenase VII (Sigma Aldrich, USA) was performed in accordance with the study of Rosenberg et al. [23]. Briefly, rats were placed on a stereotaxic frame under anesthesia.2ul collagenase VII (0.25 U/ul) was slowly injected into the right basal ganglia (stereotaxic coordinates were 1.0 mm posterior, 3.0 mm lateral, and 5.8 mm below the horizontal plane of bregma). Then, the microsyringe was left in place for an additional 10 min to prevent backflow and the cranial burr hole was sealed with bone wax. The sham-operated rats received an insertion of microsyringe without injection. During all surgical procedures, the heart rate, blood pressure and body temperature were monitored all the time, and the rectal temperature was maintained at 37 ˚C.

2.4. Neurological function assessment and measurement of brain water content

Neurological function was assessed using corner tests and forelimb placement tests, as described previously [24]. The wet weight of the brain was immediately obtained by an electric analytic balance, while the dry weight was obtained after the brain was dried in an electric oven at 100 ˚C for 24 h. Brain water content was assessed as: (wet weight − dry weight)/(wet weight) × 100%.

2.5. Immunohistochemistry (IHC) analysis

After the brains were fixed by 4% paraformaldehyde for 48 h, they were dehydrated in graded ethanol and vitrificated by xylene. Tissues were paraffin-embedded and sectioned at 4 μm thickness.

For immunohistochemistry staining, the slices were first dewaxed and re-hydrated, then incubated with 3% H2O2 at room temperature for 10 min, followed by washing with PBS. After washing the slices three times, antigen retrieval was performed, and the slices were blocked with 10% non-immune goat serum for 20 min and incubated with Iba1 antibody (1:200;Abcam) overnight at 4 ˚C. After washing with PBS, the slices were incubated with biotinylated goat anti-rabbit IgG secondary antibody for 20 min, and the Strept Avidin Biotin-peroxidase Complex (SABC) reagent was added for 10 min at 37 ˚C. Finally, the immunoreactivity was detected using 3,3-diaminobenzidine (DAB), followed by re-staining with hematoxylin.

2.6. TUNEL staining

TUNEL staining by an in-situ cell death detection kit (Roche, Germany) was performed as described previously [25]. For co-staining of NeuN and TUNEL, the sections were first incubated with NeuN antibody (1:200, Abcam), followed by TUNEL reagents according to the manufacturer's instructions.

2.7. Cell culture and treatment

Microglial BV2 cells were purchased from the Cell Resource Center of the Peking Union Medical College (China) and cultured in DMEM-HG with 10% heat-inactivated fetal bovine serum (Gibco, New Zealand.). Hippocampal neuronal HT22 cells were obtained from the Bena Culture Collection (China) and cultured in DMEM/F-12 supplemented with 10% fetal bovine serum (Gibco, New Zealand). To simulate ICH conditions *in vitro*, cells were exposed to hemin (MedChemExpress, China). To determine the appropriate condition of hemin for the treatment, cells were incubated with hemin at 20 μM, 40 μM, 60 μM, 80 μM and 100 μM. In the subsequent experiments, treatment with 60 μM hemin for 24 h was selected as an *in vitro* model of ICH.

2.8. Cell transfection

MiR-152 mimics and inhibitors, nonsense sequence for miRNA negative control (miR-NC), and siRNA against TXNIP (si-TXNIP) were purchased from Genepharma (China). BV2 cells were transfected with Lipofectamine 3000 (Invitrogen, USA) according to the manufacturer's protocol. The RNA oligonucleotide sequences are listed in Supplementary Table 1.

2.9. RNA extraction and reverse transcription quantitative PCR (RT-qPCR)

Total RNA was extracted from tissues and cells using TRIzol™ (Invitrogen, USA), according to the manufacturer's protocol. RNA was reverse-transcribed to cDNA using a reverse transcription kit (Takara Bio, China), and cDNA was amplified using a Lightcycler 96 (Roche, Germany) with a SYBR Green PCR kit (Takara Bio, China). Primer sequences are listed in Supplementary Table 2.

2.10. Cytokine ELISA assay

Cytokines, including rat and mouse IL-1β, TNF-α, IL-6, and IL-18, were measured by ELISA Array Kits according to the manufacturer's protocol. These kits were purchased from R&D Systems (USA) and Bio-SWAMP (China).

2.11. Co-immunoprecipitation

After treatment, the cells were collected, then lysed on ice for 1 h and centrifuged at 12,000*g* and 4 °C for 30 min. Approximately 500–1000 μg of protein was supplemented with 1 μg of the indicated antibody overnight at 4 °C, with agitation. Protein A beads (Beyotime Company, China) were added and incubated overnight at 4 °C with agitation. After washing three times, the immunoprecipitated proteins were solubilized with the loading buffer, and subsequently assessed by Western blotting.

2.12. Western blotting

After treatment, brain samples and cells were collected and lysed with RIPA lysis buffer (Beyotime Company, China). Western blotting was performed as described previously [25]. The protein samples (40 μg/sample) were separated by 10% SDS-PAGE gel, and transferred onto a polyvinylidene difluoride (PVDF) membrane for 2 h. Then, the membranes were blocked with 5% nonfat milk for 1 h at 37 °C and incubated with indicated primary antibodies overnight at 4 °C. After three washes with TBST, the membranes were incubated with HRP-conjugated secondary antibodies (1:5000; ProteintechGroup) for 1 h at 37 °C. Then, the membranes were washed for another three times, and bands were visualized by enhanced chemiluminescence (ECL) and further analyzed by Image J software. The primary antibodies used as follows: anti-NLRP3, anti-TXNIP (1:500; Cell Signaling Technology), anti-cleaved caspase-1 (1:1000; ProteintechGroup) and β-actin (1:1000, Sigma).

2.13. Dual luciferase assay

BV2 cells were seeded (1×10^4 cells/well) in 24-well plates and cultured overnight, then transfected with wild-type or mutant TXNIP promoter-luciferase plasmids (0.1 μg pmirGLO-wt-TXNIP or pmirGLO-mt-TXNIP plasmid per well) using Lipofectamine 3000. The sequences of the wild-type and mutant TXNIP are listed in Supplementary Table 3. Meanwhile, the cells were co-transfected with either 0.4 μg miR-152 mimics or miR-NC. Luciferase activity was analyzed 48 h post-transfection using a dual-luciferase assay system (Promega, USA).

2.14. ROS measurement

The intracellular ROS in BV2 cells was detected using the non-fluorescent dye DCFH-DA (Beyotime, China). Briefly, after treatment, the cells were incubated with DCFH-DA for 30 min at 37 °C in the dark. The fluorescence was measured using a multi-function microplate reader with 488 nm excitation and 525 nm emission.

2.15. CCK8 and LDH assay

We estimated cell viability using the CCK8 kit (Dojindo, Japan) following the manufacturer's instructions. Briefly, after treatment, 10 μL of CCK8 reagent was added to each well and the cells were incubated at 37 °C for 2 h. Optical density (OD) values were measured at 450 nm absorbance using a multi-function microplate reader.

Cytotoxicity was estimated using an LDH assay kit (KeyGen, China) according to the manufacturer's instructions. Briefly, after treatment, the cell supernatant was collected and transferred to a 96-well plate for testing LDH release. The OD values were obtained at 450 nm absorbance using a multi-function microplate reader.

2.16. Statistical analysis

All data are expressed as mean ± standard deviation (SD). Comparisons of normally distributed data between two groups were performed using a two-tailed Student's *t*-test. Comparisons among multiple groups were performed using one-way ANOVA followed by post hoc Newman-Keuls test. Behavioral data were analyzed using the Kruskal–Wallis test with Dunn's test for multiple comparisons. Coefficients of correlation(r) were analyzed by the Pearson correlation method. All data were analyzed using SPSS 22.0 (IBM Corp., USA) and GraphPad Prism 7.0 (GraphPad Software, USA), and p-values < 0.05 were considered statistically significant. To determine the sample size for each group, we conducted a power analysis using G * Power 3.1.9.2 software with a 5% significance level and obtained a power level > 0.9.

3. Results

3.1. MiR-152 was dysregulated in the ICH animal and cell models

To further confirm the dysregulation of miR-152 in ICH, which had been previously observed in ICH patients by means of miRNA arrays [21], we first analyzed the levels of miR-152 in ICH rats using RT-qPCR. We found that miR-152 was markedly downregulated in ICH rats (Fig. 1A). Hemin, as the decomposition product of hemoglobin, has been shown to play a critical role in ICH, and is commonly used for ICH pathogenesis studies [26]. We thus used hemin treatment on BV2 microglial cells. In such model, miR-152 dysregulation induced by hemin was consistent with the results of the animal model, and miR-152 levels were lowered by hemin in a dose-dependent (20–100 μM, 24 h) manner and a time-dependent (60 μM, 0–36 h) manner (Fig. 1B). In the subsequent experiments, we chose to perform hemin treatment at 60 μM for 24 h. Next, we used Iba1 + cell number and serum IL-1β, TNF-α and IL-6 levels as indicators to monitor the accompanying neuroinflammation in ICH rats (Fig. 1C and D). Interestingly, we found that miR-152 levels in the perihematoma region tissue were correlated with the changes in inflammatory indicators, including IL-1β, TNF-α, and IL-6 (Fig. 1E). Collectively, our results showed that miR-152 levels were downregulated in ICH models, both *in vivo* and *in vitro*, which might be involved in the neuroinflammation following ICH.

3.2. MiR-152 inhibited hemin-induced inflammatory response and ROS generation in BV2 cells, and protected the co-cultured HT22 neuronal cells in vitro

To explore the role of miR-152 in hemin-induced inflammation *in*

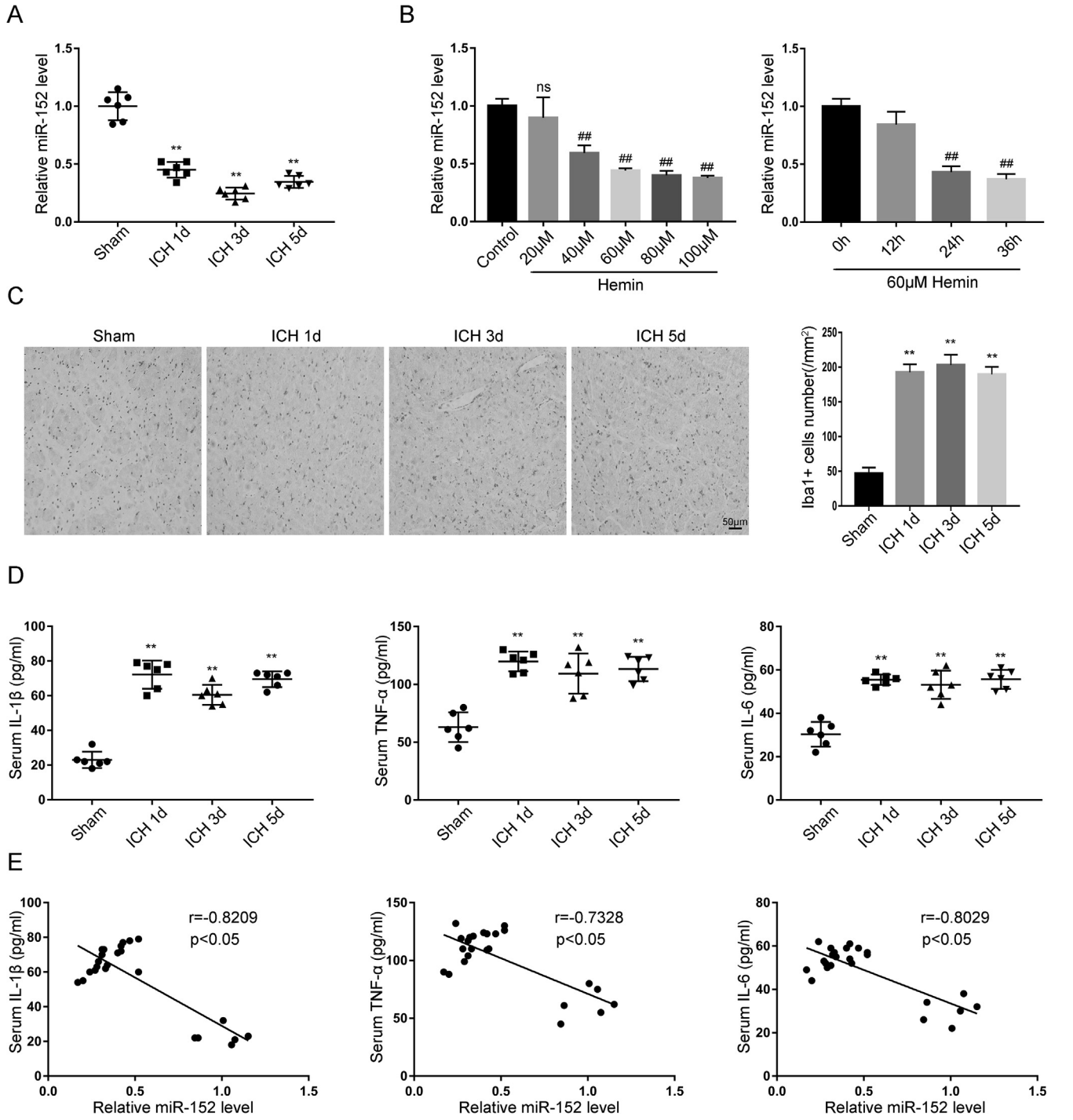

Fig. 1. MiR-152 was dysregulated in the ICH animal and cell models. (A) RT-qPCR assays for miR-152 in rat perihematomal tissue on days 1, 3 and 5 after ICH as compared with sham group (n = 6 each). Each point represents one sample, and the horizontal line indicates the mean value. (B) RT-qPCR assays for miR-152 in BV2 cells under hemin-stimulation as compared with control group (n = 3 each). (C) Immunohistochemistry for Iba1 in rat perihematomal tissue as compared with sham group. (D) Elisa assays for serum IL-1β, TNF-α and IL-6. (E) Correlations between miR-152 levels and serum inflammatory cytokines using the same samples from ICH rats and sham-operated rats. **p < 0.01 compared with sham group; ##p < 0.01 compared with BV2 control group.

vitro, we transfected BV2 microglial cells with miR-152 mimics, inhibitors, or miR-NC (Fig. 2A). Consistent with previous studies, hemin exposure significantly elevated the secretion of pro-inflammatory cytokines in BV2 cells [25]; however, overexpressing miR-152 by mimics effectively decreased the levels of pro-inflammatory cytokines, while miR-152 inhibitors further increased them (Fig. 2B). Oxidative stress induced by blood cell components is known to contribute to the severity of ICH [27]. Therefore we next analyzed the generation of ROS in BV2 cells after the different treatments. As shown in Fig. 2C, overexpression of miR-152 reduced hemin-induced ROS generation and inhibition of miR-152 led to aggravation.

To detect the neurotoxic potential of the hemin-induced microglia, the conditioned medium of transfected and hemin-treated BV2 cells was added to neuronal HT22 cells. HT22 cell viability was measured by the CCK8 assay. The hemin group showed significantly lower cell viability as compared with the control group; however, significantly higher cell

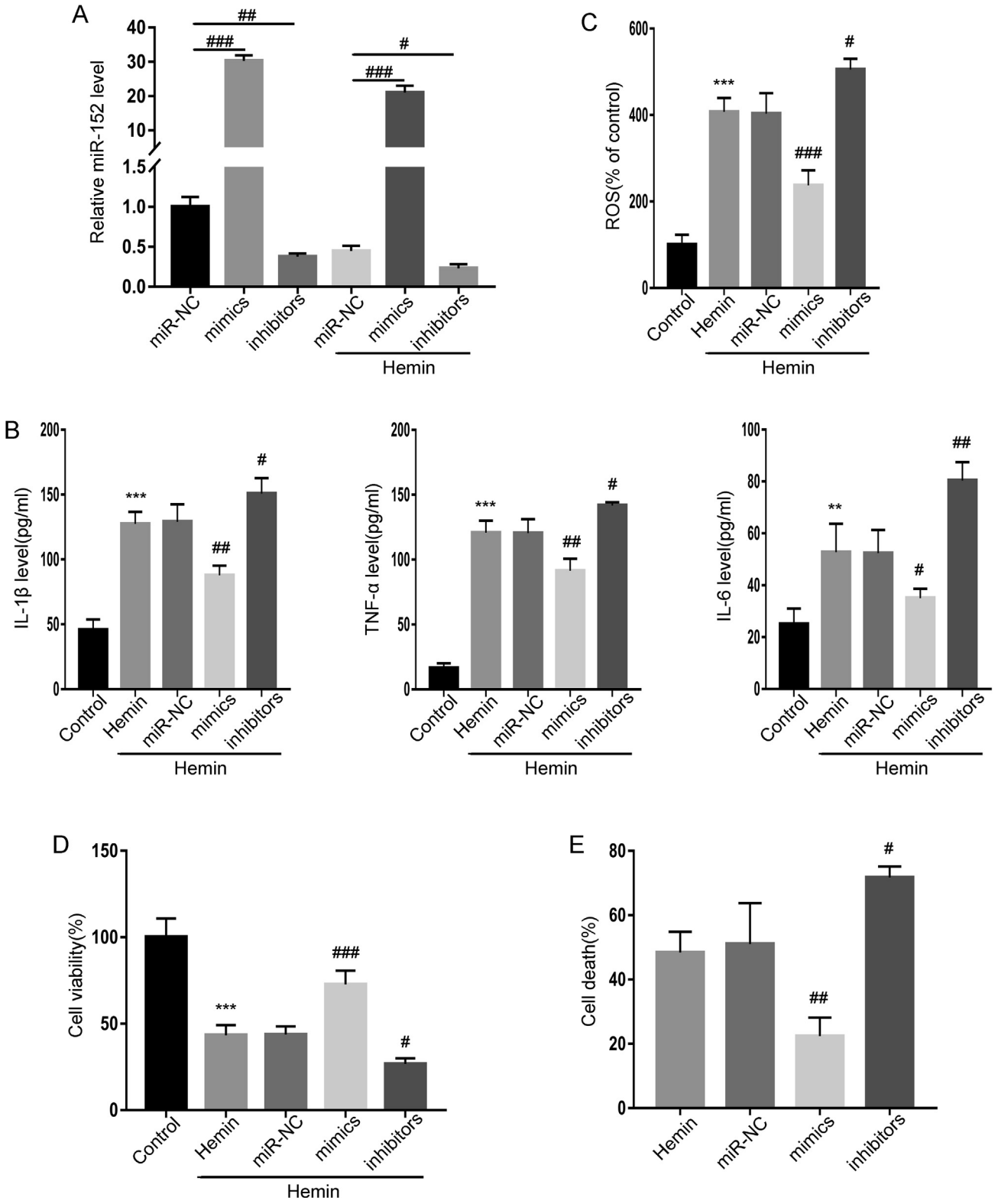

Fig. 2. MiR-152 inhibited hemin-induced inflammatory response and ROS generation in BV2 cells, and protected co-cultured HT22 neuronal cells *in vitro*. (A) RT-qPCR assays for miR-152 after transfection. (B) ELISA assays for IL-1β, TNF-α and IL-6 in supernatant of BV2 cells. (C) Levels of ROS were measured in BV2 cells. (D) Viability of HT22 cells in different groups were analyzed using CCK8 assay. (E) Cell death rates of HT22 cells in different groups were tested by LDH detection kit. $^{**}p < 0.01$, $^{***}p < 0.001$ compared with control group; $^{\#}p < 0.05$, $^{\#\#}p < 0.01$, $^{\#\#\#}p < 0.001$ compared with miR-NC transfection group under hemin stimulation.

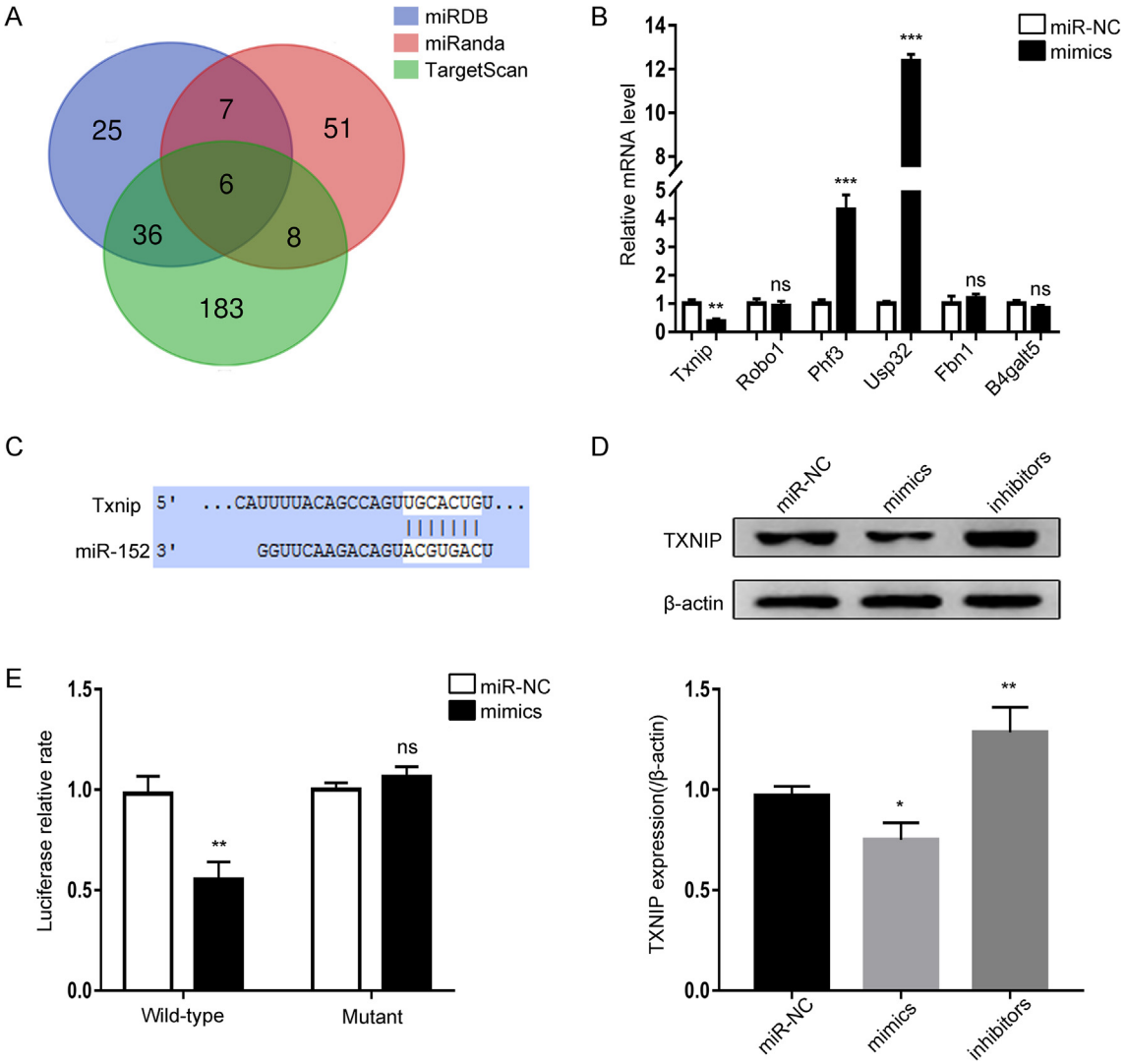

Fig. 3. The *Txnip* gene was a direct target of miR-152. (A) Predicted target genes of miR-23b using three online prediction tools, including miRDB, miRanda and TargetScan. (B) Relative mRNA level of potential target genes detected by RT-qPCR assays. (C) Target region between miR-152 and *Txnip*. (D) Western blotting of TXNIP in BV2 cells after transfection with miR-152 mimics, inhibitors or miR-NC. (E) TXNIP 3′UTR luciferase activity was assayed after BV2 cells were transfected with miR-NC or miR-152 mimics. *p < 0.05, **p < 0.01, ***p < 0.001 compared with miR-NC transfection group.

viability was observed in the miR-152 mimics-transfected group treated with hemin, as compared with the miR-NC-transfected group (Fig. 2D). Next, we examined cell death using the LDH assay. Consistently, we found that miR-152 overexpression significantly alleviated the death of co-cultured neuronal HT22 cells (Fig. 2E).

3.3. The TXNIP gene was a direct target of miR-152

To further investigate the molecular mechanisms by which miR-152 affects inflammation and oxidative stress induced by hemin, several online target-prediction tools were used, including miRDB (http://mirdb.org/), miRanda (http://www.microrna.org/microrna/home.do) and TargetScan (http://www.targetscan.org/vert_72/), we obtained a total of six candidate target genes (Fig. 3A). Among them, *Txnip* was selected for the subsequent experiments (Fig. 3B). A highly conserved pairing between the 3'UTR of *Txnip* and the seed sequence of miR-152 was observed (Fig. 3C).

To assess the effect of miR-152 on TXNIP, we transfected BV2 cells with miR-152 mimics and inhibitors, finding that miR-152 mimics transfection lowered TXNIP protein levels, while miR-152 inhibitors transfection elevated them (Fig. 3D). Next, we precisely assessed the ability of miR-152 to inhibit TXNIP using a luciferase reporter assay. As expected, transfection with miR-152 mimics prevented luciferase expression from the wild-type, but not the mutant, TXNIP 3' UTR luciferase construct (Fig. 3E), further confirming that *Txnip* is a direct target gene of miR-152.

3.4. MiR-152 alleviated the activation of NLRP3 inflammasome by regulating TXNIP

Given that TXNIP promotes NLRP3 inflammasome activation through its binding to NLRP3 [28], we then investigated the role of miR-152 on NLRP3 inflammasome in ICH *in vitro*. First, we analyzed the protein level of cleaved caspase-1, finding that hemin exposure increased its expression in BV2 cells, which was significantly reduced by miR-152 mimics (Fig. 4A). The NLRP3 inflammasome effectors, IL-1β and IL-18, are initially processed as the inactive forms pro-IL-1β and pro-IL-18, which are cleaved by active caspase-1 to produce the mature forms [29]. We observed that miR-152 effectively inhibited IL-1β and IL-18 secretion in BV2 cells under hemin treatment (Fig. 4B). Collectively, these data demonstrated that miR-152 suppressed the activation of NLRP3 inflammasome *in vitro*.

Next, we tried to further explore the specific mechanism by which miR-152 inhibited the activation of NLRP3 inflammasome.

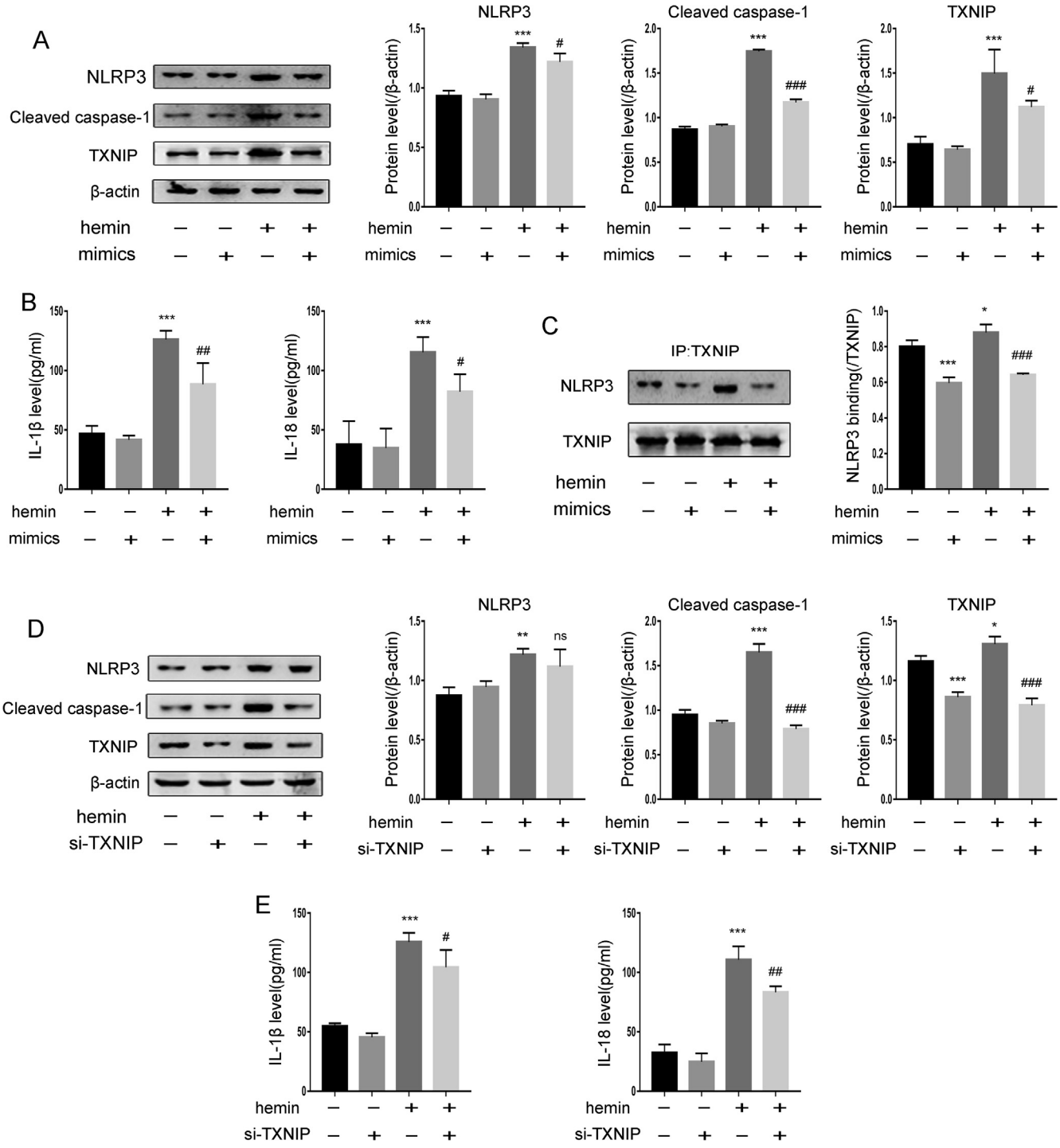

Fig. 4. MiR-152 alleviated the activation of NLRP3 inflammasome by regulating TXNIP. (A) Western blotting for NLRP3, cleaved caspase-1 and TXNIP in BV2 cells of different groups. (B) ELISA assays for inflammasome effectors IL-1β and IL-18 in supernatant of BV2 cells. (C) Co-immunoprecipitation for NLRP3 and TXNIP in BV2 cells of different groups. (D) Western blotting for NLRP3, cleaved caspase-1 and TXNIP in BV2 cells after transfection with si-TXNIP. (E) ELISA assays for IL-1β and IL-18 in supernatant of BV2 cells after transfection with si-TXNIP. *p < 0.05, **p < 0.01, ***p < 0.001 compared with control group; #p < 0.05, ##p < 0.01, ###p < 0.001 compared with hemin group.

Interestingly, co-immunoprecipitation analysis indicated that hemin treatment enhanced the binding of TXNIP to NLRP3, while miR-152 blocked it (Fig. 4C). Moreover, knockdown of TXNIP by siRNA resulted in a decrease of cleaved caspase-1 level and IL-1β, IL-18 secretion, with no changes in NLRP3 levels, compared with the si-control transfected group under hemin treatment (Fig. 4D and E). Taken together, these results suggest that miR-152 alleviates the activation of NLRP3 inflammasome by regulating TXNIP.

3.5. MiR-152 ameliorated neurodeficits, brain injury, and neuronal death in ICH rats

To validate the effect of miR-152 on ICH rats, we overexpressed miR-152 *in vivo* using lentivirus infection (Fig. 5A). As shown in Fig. 5B, miR-152 markedly alleviated ICH-induced neurodeficits, as revealed by corner tests and forelimb placement experiments. In accordance with these behavioral assessments, miR-152 significantly reduced brain

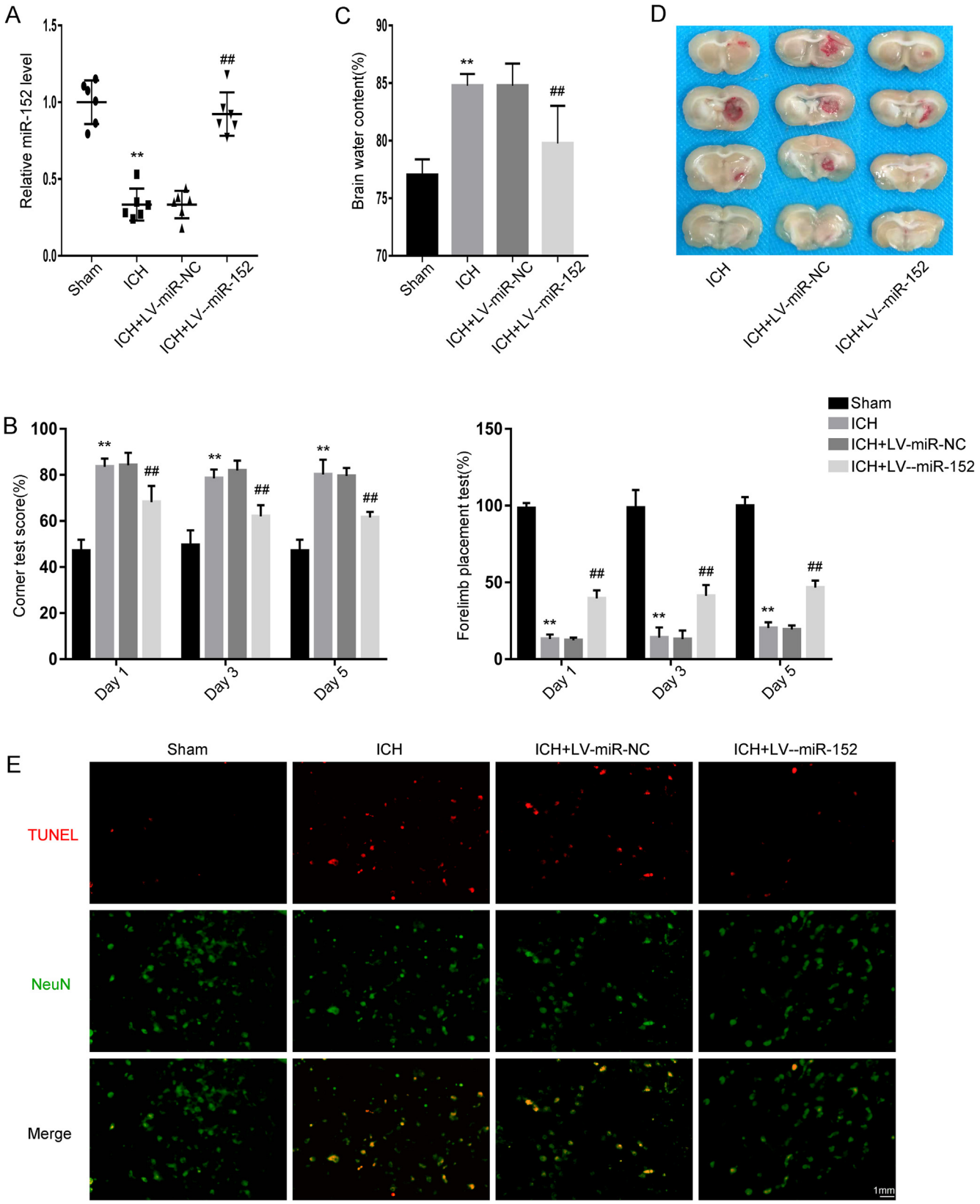

Fig. 5. MiR-152 ameliorated neurodeficits, brain injury, and neuronal death in ICH rats. (A) RT-qPCR assays for miR-152 in rat perihematomal tissue as compared with sham group (n = 6 each). Each point represents one sample, and the horizontal line indicates the mean value. (B)Corner tests and forelimb placement tests were performed for assessing neurodeficits on days 1, 3 and 5 after ICH (n = 6 each). (C) Brain water content was measured on day 3 after ICH (n = 6 each). (D) Representative brain sections from each group on day 3 after ICH were shown. (E) Apoptotic neuronal cells were detected by co-staining of NeuN and TUNEL. **p < 0.01 compared with sham group; ##p < 0.01 compared with ICH + LV-miR-NC group.

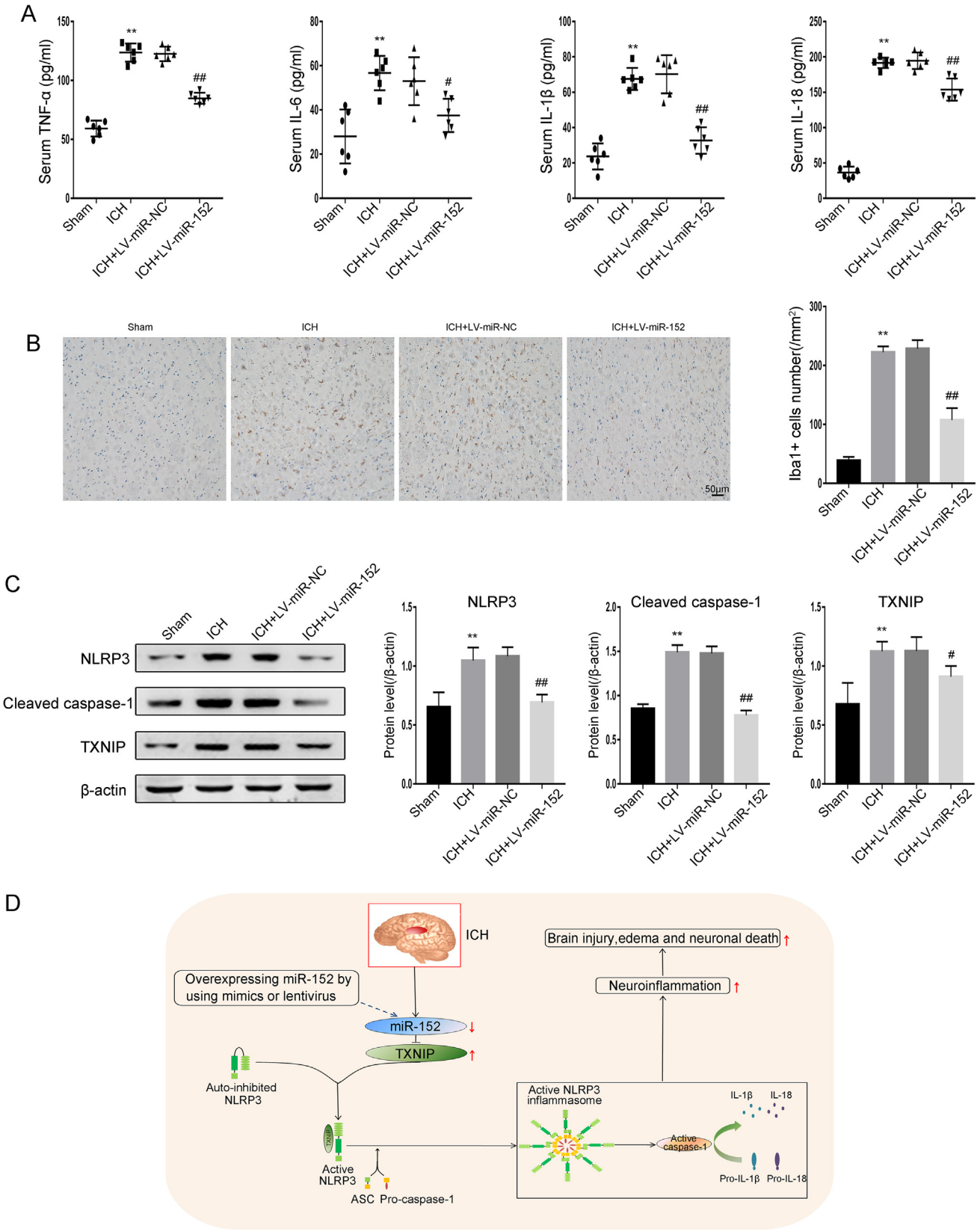

Fig. 6. MiR-152 suppressed ICH-induced neuroinflammation and NLRP3 inflammasome activation *in vivo*. (A) Elisa assays for serum TNF-α, IL-6, IL-1β and IL-18 (n = 6 each). Each point represents one sample, and the horizontal line indicates the mean value. (B) Immunohistochemistry for Iba1 in rat perihematomal region. (C) Western blotting for NLRP3, cleaved caspase-1 and TXNIP in rat perihematomal tissue. (D) Schematic representation of miR-152 protection on ICH. ICH decreased the level of miR-152, resulting in brain injury, edema and neuronal death via promotion of TXNIP-mediated NLRP3 inflammasome activation and aggravation of neuroinflammation. These post-ICH pathological changes were effectively alleviated by overexpressing miR-152 using mimics transfection *in vitro* or lentivirus induction *in vivo*. $^{**}p < 0.01$ compared with sham group; $^{\#}p < 0.05$, $^{\#\#}p < 0.01$ compared with ICH + LV-miR-NC group.

edema and hematoma size (Fig. 5C and D). In addition, NeuN and TUNEL co-staining showed that overexpression of miR-152 significantly decreased ICH-induced neuronal death (Fig. 5E). Collectively, these results suggest that miR-152 plays a protective role against ICH *in vivo*.

3.6. MiR-152 suppressed ICH-induced neuroinflammation and NLRP3 inflammasome activation in vivo

Accumulating evidence indicates that neuroinflammation plays a vital role in the pathogenesis of ICH [30]. To determine the role of miR-152 on neuroinflammation following ICH, we detected the serum levels of pro-inflammatory cytokines by ELISA, and found that miR-152 significantly reduced the elevated TNF-α and IL-6 levels caused by ICH (Fig. 6A). Moreover, miR-152 overexpression markedly inhibited the number of Iba1+ inflammatory cells in the perihematoma area (Fig. 6B). We further investigated the effect of miR-152 on TXNIP-NLRP3 inflammasome:Immunoblotting results showed that miR-152 decreased TXNIP and cleaved caspase-1 levels (Fig. 6C). Moreover, the NLRP3 inflammasome effectors, mainly serum IL-1β and IL-18, were reduced by miR-152 overexpression (Fig. 6A), further demonstrating the suppression of inflammasome activation by miR-152. Overall, our results imply that miR-152 protects against ICH by suppressing neuroinflammation through inhibiting TXNIP-mediated NLRP3 inflammasome activation (Fig. 6D).

4. Discussion

Increasing evidence has shown that miRNAs exert diverse biological effects in the brain, and that dysregulation of the levels of specific miRNAs is involved in the occurrence and progression of brain injury [31,32]. In the previous miRNA array data, we identified miR-152 as significantly downregulated in the serum of ICH patients compared with controls [21]. Since miR-152 has not been explored in ICH before, we focused on its dysregulation in the pathogenesis of ICH. Consistently with the miRNA array results, we observed a marked decrease of miR-152 levels in the collagenase VII-induced ICH rat model, and such decrease was further confirmed by the results of hemin-stimulation of BV2 cells *in vitro*. Moreover, we observed a negative correlation between miR-152 levels and inflammatory parameters in ICH rats. Collectively, these results further suggest that dysregulation of miR-152 is involved in the progression of ICH, an effect which may be specifically related to ICH-induced inflammation.

Neuroinflammation mainly arises from blood components, such as hemin, fibrin, and thrombin [33,34]. These stimuli can trigger microglia activation, promote the secretion of pro-inflammatory cytokines via TLR4/nuclear factor-κB (NF-κB) signaling, and enhance neutrophil and monocyte infiltration [35–37], which can in turn further aggravate ICH-induced brain injury. These excessive inflammatory responses are believed to be modulated by miRNAs. In our study, overexpression of miR-152 by mimics transfection significantly decreased hemin-induced pro-inflammatory cytokines IL-1β, TNF-α, and IL-6 in microglial cells *in vitro*. Consistently, overexpression of miR-152 in ICH rats by intraventricular administration of lentivirus markedly reduced serum IL-1β, TNF-α, and IL-6 levels, together with the number of Iba1+ inflammatory cells. These results are in line with the anti-inflammatory properties of miR-152 observed in other diseases [18,19]. Oxidative stress is another major mechanisms contributing to ICH outcomes [38] and anti-oxidant treatments have been shown to be effective in protecting against ICH [39,40]. Our results obtained with a DCFH-DA probe showed that miR-152 significantly reduced hemin-induced ROS generation in BV2 cells.

Neurons are the basic structural and functional units of the nervous system, and recent studies revealed that suppression of neuronal apoptosis may improve the prognosis of ICH [26,41]. In our studies, LV-miR-152 alleviated ICH-induced neuronal death in the perihematomal region *in vivo*. Moreover, overexpression of miR-152 in BV2 cells protected co-cultured neuronal cells from hemin-induced injury *in vitro*, which further confirmed the indirect protective role exerted on neurons by miR-152. Collectively, our results suggest that miR-152 exerts anti-inflammatory and anti-oxidant effects in the ICH microenvironment, thus protecting neurons from injury.

MiRNAs are well known to perform their biological functions by downregulating target genes. To further understand the mechanisms by which miR-152 acts on ICH, we identified putative target genes by using several online-prediction tools, such as TargetScan, miRDB, and miRanda. TXNIP, a member of the α-arrestin protein superfamily, was identified as a novel target of miR-152, and such targeting was further verified by a luciferase reporter assay. Recent studies have shown that TXNIP is an endogenous inhibitor of the antioxidant thioredoxin and a ROS sensor. Once ROS levels increase due to external stimuli, TXNIP time-dependently dissociates from thioredoxin, then links with NLRP3, leading to NLRP3 inflammasome activation [42,43]. Thus, our data suggests that downregulation of TXNIP by miR-152 may be related to the reduction of ROS levels.

It is known that NLRP3 inflammasome is a cytoplasmic protein complex, playing a critical role in promoting neuroinflammation and brain injury after ICH [44]. Activation of the NLRP3 inflammasome pathway consists of two steps: the first signal is the increased transcription of the inflammasome gene components, then the second is the assembly of NLRP3, ASC, and pro-caspase-1 into an oligomer complex and the activation of the NLRP3 inflammasome, which is enhanced by TXNIP. Once the NLRP3 inflammasome is activated, pro-caspase-1 is in turn activated, and specifically cleaves pro-IL-1β and pro-IL-18 to produce the respective active forms, which are then released from the cells and promote the inflammatory response [43,45]. In our studies, hemin treatment was observed to enhance the interaction of TXNIP and NLRP3, which was blocked by miR-152. Moreover, miR-152 suppressed NLRP3 inflammasome activation by targeting TXNIP in ICH both *in vivo* and *in vitro*, as revealed by the decrease in cleaved-caspase-1 expression and secreted IL-1β and IL-18 levels. The subsequent experiments using a siRNA against TXNIP further verified these effects. However, in this study, TXNIP knockdown did not affect the levels of NLRP3. These results are in line with previous studies showing that the inhibition of TXNIP attenuated inflammasome activation, by affecting the interaction between TXNIP and NLRP3, rather than by altering the expression of NLRP3 or ASC [46,47]. Together, our results demonstrate that miR-152 alleviates neuroinflammation in ICH by inhibiting TXNIP-mediated NLRP3 inflammasome activation.

More importantly, the protective role of miR-152 on ICH was further confirmed by the assessment of neurological function *in vivo*. Our findings demonstrated that miR-152 significantly improved neurological function in ICH rats, as revealed by corner tests and forelimb placing tests. Initial post-ICH hematoma enlargement and secondary perihematoma edema were demonstrated to result in the deterioration of neurological function and poor prognosis [48,49]. In the present study, overexpressing miR-152 effectively relieved the symptoms of hematoma and edema caused by ICH in rats. Collectively, our results imply that miR-152 exerts protective effects on ICH.

However, a few limitations of the present study should be noted. First, we used collagenase VII-induced ICH *in vivo*, a widely used animal model of ICH [23,50] which, however, cannot completely mimic the pathophysiological process occurring in ICH patients. Second, we used the BV2 microglial cell line and the HT22 neuronal cell line for the study of microglia-neuron interaction after ICH. These cell lines have been previously investigated by other researchers to study ICH *in vitro* [30,51] but the study of such derived cell lines cannot entirely replace the investigation of primary cells. In addition, our results showed that the overexpression of miR-152 in BV2 cells exerted an indirect protective effect on co-cultured neurons by targeting TXNIP-mediated NLRP3 inflammasome, but whether miR-152 also has a direct protective effects is unclear, and whether pyroptosis, a form of caspase 1-dependent cell death [29,52], is involved in the modulation of miR-152

is still unknown. Hence, such hypotheses should be further explored.

In conclusion, the present study demonstrates that miR-152 inhibited TXNIP-mediated NLRP3 inflammasome activation to alleviate neuroinflammation and brain injury in ICH. The results provide new insight for the development of ICH therapies, by indicating miR-152 as a potential therapeutic target.

Author contributions

Liuting Hu performed the experiments, obtained the data and drafted the original paper; all authors analyzed and interpreted the data; Zhiyi He designed the study and examined the paper. All authors agree to be accountable for the work content.

Funding

This work was supported by the National Natural Science Foundation of China [grant number 81571120].

CRediT authorship contribution statement

Liuting Hu: Validation, Formal analysis, Investigation, Data curation, Writing - original draft, Writing - review & editing, Visualization. **Heyu Zhang:** Validation, Formal analysis, Data curation. **Bingyang Wang:** Validation, Formal analysis, Data curation. **Qiang Ao:** Validation, Resources, Formal analysis. **Zhiyi He:** Conceptualization, Methodology, Resources, Writing - review & editing, Supervision, Project administration, Funding acquisition.

Declaration of Competing Interest

The authors report no conflicts of interest.

Appendix A. Supplementary material

Supplementary data to this article can be found online at https://doi.org/10.1016/j.intimp.2019.106141.

References

[1] J.C. Hemphill 3rd, S.M. Greenberg, C.S. Anderson, K. Becker, B.R. Bendok, M. Cushman, et al., Guidelines for the management of spontaneous intracerebral hemorrhage: a guideline for healthcare professionals from the American Heart Association/American Stroke Association, Stroke 46 (2015) 2032–2060.
[2] M.A. Ikram, R.G. Wieberdink, P.J. Koudstaal, International epidemiology of intracerebral hemorrhage, Curr. Atherosclerosis Rep. 14 (2012) 300–306.
[3] F. Rincon, S.A. Mayer, Intracerebral hemorrhage: getting ready for effective treatments, Curr. Opin. Neurol. 23 (2010) 59–64.
[4] R.M. Babadjouni, R.E. Radwanski, B.P. Walcott, A. Patel, R. Durazo, D.M. Hodis, et al., Neuroprotective strategies following intraparenchymal hemorrhage, J. Neurointerventional Surg. 9 (2017) 1202–1207.
[5] F. Schlunk, S.M. Greenberg, The pathophysiology of intracerebral hemorrhage formation and expansion, Transl. Stroke Res. 6 (2015) 257–263.
[6] A. Shao, Z. Zhu, L. Li, S. Zhang, J. Zhang, Emerging therapeutic targets associated with the immune system in patients with intracerebral haemorrhage (ICH): from mechanisms to translation, EBioMedicine 45 (2019) 615–623.
[7] E. Mracsko, R. Veltkamp, Neuroinflammation after intracerebral hemorrhage, Front. Cell. Neurosci. 8 (2014) 388.
[8] J. Wang, Preclinical and clinical research on inflammation after intracerebral hemorrhage, Prog. Neurobiol. 92 (2010) 463–477.
[9] Y. Fang, Y. Tian, Q. Huang, Y. Wan, L. Xu, W. Wang, et al., Deficiency of TREK-1 potassium channel exacerbates blood-brain barrier damage and neuroinflammation after intracerebral hemorrhage in mice, J. Neuroinflammation 16 (2019) 96.
[10] C.H. Wu, C.C. Chen, C.Y. Lai, T.H. Hung, C.C. Lin, M. Chao, et al., Treatment with TO901317, a synthetic liver X receptor agonist, reduces brain damage and attenuates neuroinflammation in experimental intracerebral hemorrhage, J. Neuroinflammation 13 (2016) 62.
[11] C.J. Wei, Y.L. Li, Z.L. Zhu, D.M. Jia, M.L. Fan, T. Li, et al., Inhibition of activator protein 1 attenuates neuroinflammation and brain injury after experimental intracerebral hemorrhage, CNS Neurosci. Ther. 25 (2019) 1182–1188.
[12] J. Krol, I. Loedige, W. Filipowicz, The widespread regulation of microRNA biogenesis, function and decay, Nat. Rev. Genet. 11 (2010) 597–610.
[13] S. Wang, Y. Cui, J. Xu, H. Gao, miR-140-5p attenuates neuroinflammation and brain injury in rats following intracerebral hemorrhage by targeting TLR4, Inflammation 42 (2019) 1869–1877.
[14] A. Yu, T. Zhang, H. Duan, Y. Pan, X. Zhang, G. Yang, et al., MiR-124 contributes to M2 polarization of microglia and confers brain inflammatory protection via the C/EBP-alpha pathway in intracerebral hemorrhage, Immunol. Lett. 182 (2017) 1–11.
[15] S. Ge, D. Wang, Q. Kong, W. Gao, J. Sun, Function of miR-152 as a tumor suppressor in human breast cancer by targeting PIK3CA, Oncol. Res. 25 (2017) 1363–1371.
[16] Z.W. Lu, M.Y. Du, L.X. Qian, N. Zhang, J.J. Gu, K. Ding, et al., MiR-152 functioning as a tumor suppressor that interacts with DNMT1 in nasopharyngeal carcinoma, OncoTargets Therapy 11 (2018) 1733–1741.
[17] M. Friedrich, K. Pracht, M.F. Mashreghi, H.M. Jack, A. Radbruch, B. Seliger, The role of the miR-148/-152 family in physiology and disease, Eur. J. Immunol. 47 (2017) 2026–2038.
[18] Z. Ma, X. Shu, J. Huang, H. Zhang, Z. Xiao, L. Zhang, Salvia-nelumbinis naturalis formula improved inflammation in LPS stressed macrophages via upregulating MicroRNA-152, Mediators Inflamm. 2017 (2017) 5842747.
[19] T. Zhang, G. Gao, F. Chang, miR-152 promotes spinal cord injury recovery via c-jun amino terminal kinase pathway, Eur. Rev. Med. Pharmacol. Sci. 23 (2019) 44–51.
[20] X. Liu, Z. Zhan, L. Xu, F. Ma, D. Li, Z. Guo, et al., MicroRNA-148/152 impair innate response and antigen presentation of TLR-triggered dendritic cells by targeting CaMKIIalpha, J. Immunol. 185 (2010) 7244–7251.
[21] J. Wang, Y. Zhu, F. Jin, L. Tang, Z. He, Z. He, Differential expression of circulating microRNAs in blood and haematoma samples from patients with intracerebral haemorrhage, J. Int. Med. Res. 44 (2016) 419–432.
[22] F. Li, B. Yang, T. Li, X. Gong, F. Zhou, Z. Hu, HSPB8 over-expression prevents disruption of blood-brain barrier by promoting autophagic flux after cerebral ischemia/reperfusion injury, J. Neurochem. 148 (2019) 97–113.
[23] G.A. Rosenberg, S. Mun-Bryce, M. Wesley, M. Kornfeld, Collagenase-induced intracerebral hemorrhage in rats, Stroke 21 (1990) 801–807.
[24] Y. Hua, T. Schallert, R.F. Keep, J. Wu, J.T. Hoff, G. Xi, Behavioral tests after intracerebral hemorrhage in the rat, Stroke 33 (2002) 2478–2484.
[25] L. Hu, H. Zhang, B. Wang, Q. Ao, J. Shi, Z. He, MicroRNA-23b alleviates neuroinflammation and brain injury in intracerebral hemorrhage by targeting inositol polyphosphate multikinase, Int. Immunopharmacol. 76 (2019) 105887.
[26] X. Shen, L. Ma, W. Dong, Q. Wu, Y. Gao, C. Luo, et al., Autophagy regulates intracerebral hemorrhage induced neural damage via apoptosis and NF-kappaB pathway, Neurochem. Int. 96 (2016) 100–112.
[27] R.X. Xie, D.W. Li, X.C. Liu, M.F. Yang, J. Fang, B.L. Sun, et al., Carnosine attenuates brain oxidative stress and apoptosis after intracerebral hemorrhage in rats, Neurochem. Res. 42 (2017) 541–551.
[28] R. Zhou, A. Tardivel, B. Thorens, I. Choi, J. Tschopp, Thioredoxin-interacting protein links oxidative stress to inflammasome activation, Nat. Immunol. 11 (2010) 136–140.
[29] A. Wree, A. Eguchi, M.D. McGeough, C.A. Pena, C.D. Johnson, A. Canbay, et al., NLRP3 inflammasome activation results in hepatocyte pyroptosis, liver inflammation, and fibrosis in mice, Hepatology 59 (2014) 898–910.
[30] C.H. Wu, S.K. Shyue, T.H. Hung, S. Wen, C.C. Lin, C.F. Chang, et al., Genetic deletion or pharmacological inhibition of soluble epoxide hydrolase reduces brain damage and attenuates neuroinflammation after intracerebral hemorrhage, J. Neuroinflammation 14 (2017) 230.
[31] S. Freiesleben, M. Hecker, U.K. Zettl, G. Fuellen, L. Taher, Analysis of microRNA and gene expression profiles in multiple sclerosis: integrating interaction data to uncover regulatory mechanisms, Sci. Rep. 6 (2016) 34512.
[32] J. Wu, C.L. Fan, L.J. Ma, T. Liu, C. Wang, J.X. Song, et al., Distinctive expression signatures of serum microRNAs in ischaemic stroke and transient ischaemic attack patients, Thromb. Haemost. 117 (2017) 992–1001.
[33] S. Lin, Q. Yin, Q. Zhong, F.L. Lv, Y. Zhou, J.Q. Li, et al., Heme activates TLR4-mediated inflammatory injury via MyD88/TRIF signaling pathway in intracerebral hemorrhage, J. Neuroinflammation 9 (2012) 46.
[34] Y.C. Wang, Y. Zhou, H. Fang, S. Lin, P.F. Wang, R.P. Xiong, et al., Toll-like receptor 2/4 heterodimer mediates inflammatory injury in intracerebral hemorrhage, Ann. Neurol. 75 (2014) 876–889.
[35] M.D. Hammond, R.A. Taylor, M.T. Mullen, Y. Ai, H.L. Aguila, M. Mack, et al., CCR2+ Ly6C(hi) inflammatory monocyte recruitment exacerbates acute disability following intracerebral hemorrhage, J. Neurosci.: Off. J. Soc. Neurosci. 34 (2014) 3901–3909.
[36] Q. Ma, A. Manaenko, N.H. Khatibi, W. Chen, J.H. Zhang, J. Tang, Vascular adhesion protein-1 inhibition provides antiinflammatory protection after an intracerebral hemorrhagic stroke in mice, J. Cerebral Blood Flow Metabolism: Off. J. Int. Soc. Cerebral Blood Flow Metabolism 31 (2011) 881–893.
[37] X. Lan, X. Han, Q. Li, Q. Li, Y. Gao, T. Cheng, et al., Pinocembrin protects hemorrhagic brain primarily by inhibiting toll-like receptor 4 and reducing M1 phenotype microglia, Brain Behav. Immun. 61 (2017) 326–339.
[38] J. Aronowski, X. Zhao, Molecular pathophysiology of cerebral hemorrhage: secondary brain injury, Stroke 42 (2011) 1781–1786.
[39] H. Wu, T. Wu, X. Han, J. Wan, C. Jiang, W. Chen, et al., Cerebroprotection by the neuronal PGE2 receptor EP2 after intracerebral hemorrhage in middle-aged mice, J. Cerebral Blood Flow Metabolism: Off. J. Int. Soc. Cerebral Blood Flow Metabolism 37 (2017) 39–51.
[40] N. Singh, Y. Bansal, R. Bhandari, L. Marwaha, R. Singh, K. Chopra, et al., Resveratrol protects against ICV collagenase-induced neurobehavioral and biochemical deficits, J. Inflamm. 14 (2017) 14.
[41] J. Shen, T. Zhou, H. Li, W. Li, S. Wang, Y. Song, et al., Cab45s inhibits neuronal apoptosis following intracerebral hemorrhage in adult rats, Brain Res. Bull. 143 (2018) 36–44.
[42] X. Ye, D. Zuo, L. Yu, L. Zhang, J. Tang, C. Cui, et al., ROS/TXNIP pathway

contributes to thrombin induced NLRP3 inflammasome activation and cell apoptosis in microglia, Biochem. Biophys. Res. Commun. 485 (2017) 499–505.
[43] J.M. Abais, M. Xia, G. Li, Y. Chen, S.M. Conley, T.W. Gehr, et al., Nod-like receptor protein 3 (NLRP3) inflammasome activation and podocyte injury via thioredoxin-interacting protein (TXNIP) during hyperhomocysteinemia, J. Biol. Chem. 289 (2014) 27159–27168.
[44] Q. Ma, S. Chen, Q. Hu, H. Feng, J.H. Zhang, J. Tang, NLRP3 inflammasome contributes to inflammation after intracerebral hemorrhage, Ann. Neurol. 75 (2014) 209–219.
[45] V. Bharti, H. Tan, H. Zhou, J.F. Wang, Txnip mediates glucocorticoid-activated NLRP3 inflammatory signaling in mouse microglia, Neurochem. Int. 104564 (2019).
[46] B. Luo, B. Li, W. Wang, X. Liu, Y. Xia, C. Zhang, et al., NLRP3 gene silencing ameliorates diabetic cardiomyopathy in a type 2 diabetes rat model, PLoS ONE 9 (2014) e104771.
[47] Y.J. Park, S.J. Yoon, H.W. Suh, D.O. Kim, J.R. Park, H. Jung, et al., TXNIP deficiency exacerbates endotoxic shock via the induction of excessive nitric oxide synthesis, PLoS Pathog. 9 (2013) e1003646.
[48] J. Wang, G. Wang, J. Yi, Y. Xu, S. Duan, T. Li, et al., The effect of monascin on hematoma clearance and edema after intracerebral hemorrhage in rats, Brain Res. Bull. 134 (2017) 24–29.
[49] B. Volbers, S. Herrmann, W. Willfarth, H. Lucking, S.P. Kloska, A. Doerfler, et al., Impact of hypothermia initiation and duration on perihemorrhagic edema evolution after intracerebral hemorrhage, Stroke 47 (2016) 2249–2255.
[50] J.A. Chesney, T. Kondoh, J.A. Conrad, W.C. Low, Collagenase-induced intrastriatal hemorrhage in rats results in long-term locomotor deficits, Stroke 26 (1995) 312–316 discussion.
[51] Z. Yang, T. Zhao, Y. Zou, J.H. Zhang, H. Feng, Curcumin inhibits microglia inflammation and confers neuroprotection in intracerebral hemorrhage, Immunol. Lett. 160 (2014) 89–95.
[52] T. Bergsbaken, S.L. Fink, B.T. Cookson, Pyroptosis: host cell death and inflammation, Nat. Rev. Microbiol. 7 (2009) 99–109.